

# Automated classification of transient contamination in stationary acoustic data

Christopher J. Bahr · Todd Schultz

the date of receipt and acceptance should be inserted later

**Abstract** An automated procedure for the classification of transient contamination of stationary acoustic data is proposed and analyzed. The procedure requires the assumption that the stationary acoustic data of interest can be modeled as a band-limited, Gaussian random process. It also requires that the transient contamination be of higher variance than the acoustic data of interest. When these assumptions are satisfied, it is a blind separation procedure, aside from the initial input specifying how to subdivide the time series of interest. No a priori threshold criterion is required. Simulation results show that for a sufficient number of blocks, the method performs well, as long as the occasional false positive or false negative is acceptable. The effectiveness of the procedure is demonstrated with an appli-

---

Christopher J. Bahr

Aeroacoustics Branch, NASA Langley Research Center, Hampton, Virginia, USA

Tel.: 1-757-864-9162

E-mail: christopher.j.bahr@nasa.gov

ORCID: 0000-0002-3095-4265

Todd Schultz

Boeing Test & Evaluation, The Boeing Company, Seattle, Washington, USA

cation to experimental wind tunnel acoustic test data which are contaminated by hydrodynamic gusts.

**Keywords** binary classification · noise contamination · unsupervised methods

### Nomenclature

$B$  = normalized signal bandwidth

$K$  = Kullback-Leibler divergence

$M$  = Mach number

$N$  = number of samples in a block of data

$n$  = sample index

$P$  = probability distribution function

$p$  = probability density function

$Q$  = probability distribution function, estimate of  $P$

$q$  = probability density function, estimate of  $p$

$y_n$  = individual sample in a block of data

$\alpha$  = gamma distribution shape parameter

$\beta$  = gamma distribution scale parameter

$\Gamma$  = gamma function

$\gamma$  = incomplete gamma function

$\nu$  = effective degrees of freedom for signal of block size  $N$

$\sigma^2$  = variance of a block of data

$\chi_N^2$  = sum of the squares of the samples in a block of data

## 1 **1 Introduction**

2 In aeroacoustic wind tunnel testing, experimentalists often seek to measure acous-  
3 tic signals, which can be modeled as band-limited, stationary random processes.  
4 The unfortunate reality for some experimental setups is that the acoustic signal  
5 of interest will be measured along with some form of contamination. For example,  
6 in an open-jet and acoustically-treated wind tunnel facility, the contamination ob-  
7 served by a microphone may manifest as either stationary pressure fluctuations  
8 generated by facility acoustic sources, or transient pressure fluctuations generated  
9 by flow over the microphone (Soderman and Allen 2002). Stationary contamination  
10 may be mitigated through various forms of frequency domain background subtrac-  
11 tion (Humphreys et al. 1998; Bahr and Horne 2017). However, such techniques are  
12 not appropriate for transient events.

13 Alternative analysis methods are required to classify and separate time do-  
14 main contamination. While manual inspection of data is an option, this is usually  
15 impractical due to the large volume of data involved. Simple methods such as  
16 Chauvenet’s criterion (Coleman and Steele 1999) allow for the classification of  
17 outliers in Gaussian-distributed random data. Advanced methods are available for  
18 analyzing more complicated scenarios as shown in Aggarwal (2017) and Hawkins  
19 (1980), for example. However, rejection of individual samples may not be beneficial  
20 in time series analysis, as continuous blocks of data are usually required for sub-  
21 sequent spectral processing. Common block properties, as discussed subsequently,  
22 do not follow a Gaussian distribution and thus do not lend themselves to analysis  
23 with basic tools. More advanced tools, to the authors’ knowledge, have not been

24 developed with this specific type of classification problem in mind wherein a priori  
 25 data assumptions and thresholding parameters are minimized.

26 This work presents a tailored, alternative method which requires minimal in-  
 27 put aside from the parameters to subdivide a given time series of interest into  
 28 individual blocks, sized according subsequent analysis needs. The identification  
 29 and separation methodology has a well-defined parameter for classifying transient  
 30 data, which should be valid as long as the underlying assumptions are approxi-  
 31 mately obeyed. It is assumed that the acoustic signal of interest is a stationary,  
 32 zero mean, Gaussian random process. With this assumption, the block variances  
 33 can be modeled using a gamma distribution. It is subsequently assumed that the  
 34 acoustic data of interest are of lower variance than transient contaminating data.  
 35 Both mean- and median-based distributions are computed and compared, making  
 36 the method robust to extreme values. The detailed development of this classifica-  
 37 tion technique is given in the following section. Subsequent sections evaluate the  
 38 classification performance with both simulated and experimental data. These are  
 39 followed by recommendations developed from the results.

## 40 **2 Theoretical Development**

41 The first assumption required for this transient classification procedure is that the  
 42 underlying acoustic signal is a stationary, zero mean, Gaussian random process. If  
 43 the samples from the acoustic signal of interest,  $y$ , are truly Gaussian-distributed  
 44 random variables with zero mean and unit variance, then the sum of the squares  
 45 of a set of  $N$  samples,

$$\chi_N^2 = \sum_{n=1}^N y_n^2, \quad (1)$$

46 is a random variable, which follows a chi-square distribution with  $N$  degrees of  
 47 freedom (Zelen and Severo 1972). Eq. (2) normalizes this sum to be an unbiased  
 48 and consistent estimator of the block variance (Bendat and Piersol 2000),

$$\sigma^2 = \frac{\chi_N^2}{N-1} = \frac{1}{N-1} \sum_{n=1}^N y_n^2, \quad (2)$$

49 which also follows a chi-square distribution.

50 It is relatively easy to enforce the zero mean condition on acoustic data, either  
 51 through high-pass filtering during data acquisition or mean subtraction in post-  
 52 processing. However, the variance of the distribution for  $y$  is unknown, so a more  
 53 general distribution is necessary to model the distribution of the block variance,  
 54  $\sigma^2$ . As a generalization of the chi-square distribution, the gamma distribution can  
 55 be used (NIST 2013). The probability density function for a gamma distribution  
 56 of the block variance (with a zero location parameter) is given by

$$p(\sigma^2) = \frac{1}{\beta\Gamma(\alpha)} \left(\frac{\sigma^2}{\beta}\right)^{\alpha-1} e^{-\frac{\sigma^2}{\beta}}, \quad (3)$$

57 where  $\nu$  is the effective degrees of freedom discussed further below,  $\alpha = \nu/2$  is  
 58 the shape parameter required to relate a gamma distribution to the chi-square  
 59 distribution for data of a given bandwidth,  $\beta$  is the scale parameter and  $\Gamma$  is the  
 60 gamma function

$$\Gamma(\alpha) = \int_0^\infty t^{\alpha-1} e^{-t} dt. \quad (4)$$

61 For  $\beta = 2$ , and substituting  $\chi_N^2$  for  $\sigma^2$ , this fully collapses to the chi-square distri-  
 62 bution. This scale parameter allows a distribution fit to handle nonunity variance  
 63 of  $y$ .

64 In practice, the acoustic signal is not truly random white noise, but has a  
 65 finite bandwidth and correlation timescale. This normalized bandwidth,  $B$ , alters

66 the effective degrees of freedom,  $\nu$ , of the signal (Bendat and Piersol 2000). For  
 67 example, a block of 8192 samples of a signal, which is truly random, has a spectrum  
 68 of white noise and a bandwidth of 100%, so  $\nu = N = 8192$ . If the signal passes  
 69 through an ideal lowpass filter set to 50% of the Nyquist frequency for the sampling  
 70 rate, then  $B = 0.5$  and the effective number of degrees of freedom is  $\nu = B \times$   
 71  $N = 4096$ . This fractional, normalized bandwidth can be estimated through a  
 72 simple procedure. First, the one-sided power spectral density of the signal must  
 73 be computed. This function of frequency,  $G_{yy}(f)$ , must then be normalized such  
 74 that its peak is unity,

$$G_{yy,\text{norm}}(f) = \frac{G_{yy}(f)}{\max[G_{yy}(f)]}. \quad (5)$$

75 The average of this normalized spectral density is then computed by integrating  
 76 across the measurement bandwidth and normalizing by the integration range,

$$B = \frac{1}{f_{\max}} \int_0^{f_{\max}} G_{yy,\text{norm}}(f) \, df. \quad (6)$$

77 The normalized bandwidth can take a wide range of values. With the experimental  
 78 data discussed later in this work, for example, it is found to be on the order of  
 79  $10^{-3}$  for data acquired at a high sampling rate but dominated by low frequency  
 80 spectral content.

81 With the effective degrees of freedom and, thus, the shape parameter of a  
 82 distribution fit derived from the signal bandwidth, the scale parameter must now  
 83 be determined. An easy, if biased (Zhang 2013), estimate of  $\beta$  can be obtained  
 84 from its maximum likelihood estimator

$$\beta = \frac{\overline{\sigma^2}}{\alpha}, \quad (7)$$

85 where  $\overline{\sigma^2}$  is an estimate of the mean of the block variances. However, the mean  
 86 of the variances is sensitive to extreme variance values, which may occur when  
 87 a transient event is superimposed on the baseline Gaussian process. A statistical  
 88 parameter that is less sensitive to extreme values is necessary for computing  $\beta$ .  
 89 One such parameter is the median of the block variances. The median occurs where  
 90 the probability distribution function is 0.5. The probability distribution function  
 91 for the gamma distribution is given by

$$P(\sigma^2) = \frac{\gamma\left(\alpha, \frac{\sigma^2}{\beta}\right)}{\Gamma(\alpha)}, \quad (8)$$

92 where  $\gamma$  is the (non-normalized) incomplete gamma function (NIST 2013)

$$\gamma\left(\alpha, \frac{\sigma^2}{\beta}\right) = \int_0^{\frac{\sigma^2}{\beta}} t^{\alpha-1} e^{-t} dt. \quad (9)$$

93 The equation for the median variance is thus

$$\frac{1}{2} = \frac{\gamma\left(\alpha, \frac{\sigma_{\text{med}}^2}{\beta}\right)}{\Gamma(\alpha)}. \quad (10)$$

94 Software libraries exist for efficiently inverting  $\gamma$  for a given  $\alpha$ , thus yielding an  
 95 estimate of the median variance normalized by  $\beta$ . The experimental median vari-  
 96 ance can then be divided by this estimate, yielding an estimate of  $\beta$ . Thus, for a  
 97 given shape factor  $\alpha$ , two scale factors can be readily computed from the data.  
 98 One,  $\beta_{\text{mean}}$ , is based on the mean of the block variances and may be significantly  
 99 influenced by extreme values of block variance in the data such as may be present  
 100 with transient events. The other,  $\beta_{\text{median}}$ , is based on the median of the block vari-  
 101 ances. Note that for large sample sizes some simplifying mathematics are possible,  
 102 but avoided here to allow for small numbers of short data blocks.

103 Having two scale factors allows for the construction of two gamma distribu-  
 104 tions. These can be compared to gain some sense of the relative influence of ex-

105 treble block variances on the data set. Numerically this can be done by evaluating  
 106 the Kullback-Leibler divergence, which is one metric for comparing distributions  
 107 (Cardoso 1997). The divergence  $K$  is a measure of the information lost when prob-  
 108 ability distribution  $Q$  (or density  $q$ ) is used to estimate distribution  $P$  (or density  
 109  $p$ ). This is expressed as

$$K(p||q) = \int \ln \left[ \frac{p(\sigma^2)}{q(\sigma^2)} \right] p(\sigma^2) d(\sigma^2). \quad (11)$$

110 While, in general, this can be difficult to compute, it is greatly simplified in the  
 111 case of two gamma distributions with a common  $\alpha$ . In this case, some manipulation  
 112 yields

$$K(p||q)_{\alpha_p=\alpha_q=\alpha} = \alpha \left( \ln \beta_q - \ln \beta_p + \frac{\beta_p - \beta_q}{\beta_q} \right), \quad (12)$$

113 or, as used in this application,

$$K(p_{median}||p_{mean})_{\alpha_{median}=\alpha_{mean}=\alpha} = \alpha \left( \ln \beta_{mean} - \ln \beta_{median} + \frac{\beta_{median} - \beta_{mean}}{\beta_{mean}} \right). \quad (13)$$

114 The two distributions match when  $K$  is zero.

115 To summarize, two data distributions can be estimated. The distribution based  
 116 on the block variance mean is more sensitive to blocks with high variance, such  
 117 as those containing transient contamination, than the distribution based on the  
 118 block variance median. A metric is constructed for comparing the two distributions.  
 119 Now a procedure is proposed for determining which blocks of a given time series  
 120 to retain and which to reject. The process is illustrated in Fig. 1. It should be  
 121 noted here that for the number of blocks traditionally used in aeroacoustic wind  
 122 tunnel testing, converged data distributions are not expected. The intent of the  
 123 following procedure is to provide an automated engineering tool to locate and thus



124 exclude blocks in the time series associated with transient events, not to accurately  
125 estimate the probability distribution of the acoustic data block variance.

126 First, a given microphone time record is broken into blocks of a desired number  
127 of samples,  $N$ . This value is usually dictated by the desired spectral estimation  
128 parameters. The variance of each of these blocks is computed, and the blocks  
129 are sorted by their variance, from low to high. A minimum number of blocks is  
130 selected to automatically accept as stationary. This number of blocks is taken  
131 as the lowest-variance subset of blocks from the sorted set, and should be large  
132 enough to reduce the noise in the estimate but small enough to avoid any extreme  
133 values, or contaminated blocks. Experience with simulations suggests 20% of the  
134 total block count to be a safe selection, though a lower value was successfully used  
135 with experimental data. This subset of blocks is used to compute an autospectral  
136 density, which can be used to calculate  $\alpha$ . This can be used to compute  $\beta_{\text{mean}}$  and  
137  $\beta_{\text{median}}$ , followed by  $K$ . The next block, in order of ascending variance, is added to  
138 the active subset of blocks and the process is repeated. This continues until all of  
139 the blocks of data have been included, producing  $|K|$  as a function of the number  
140 of blocks included in the data set in order of ascending variance. The block set  
141 yielding the minimum  $|K|$  is classified as stationary. Blocks excluded from this  
142 set are classified as containing significant transient contamination. They may be  
143 subsequently excluded from processing of the stationary data of interest.

### 144 **3 Simulated Analysis**

145 A simulation study is performed to measure the performance of the transient  
146 classification procedure with data representative of experimental situations and

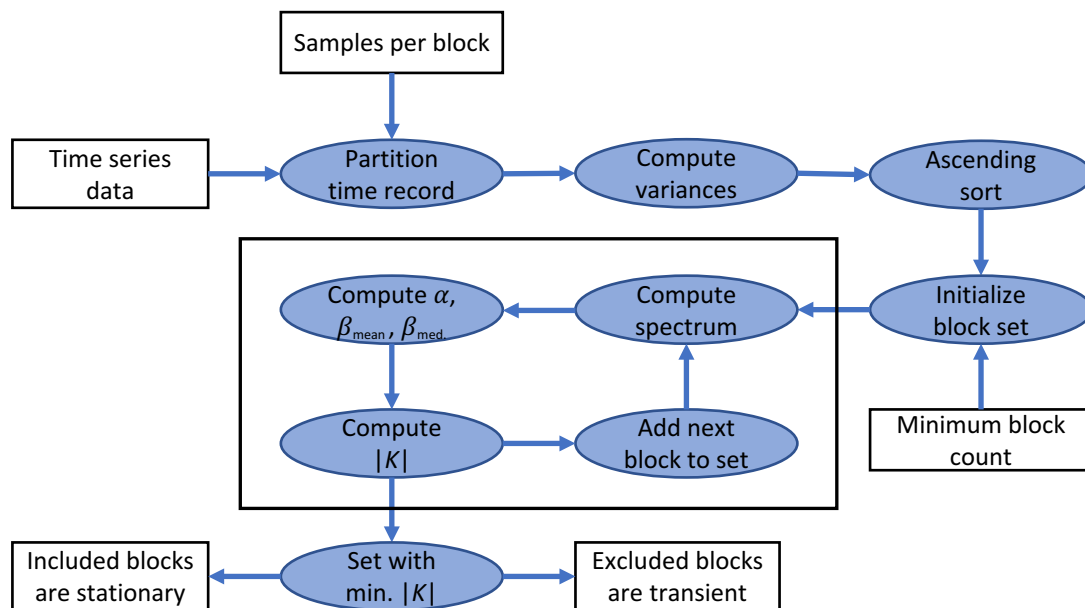


Fig. 1. Algorithm flow chart for classifying transient events.

147 parameter choices. The goal is to understand the performance of the procedure for  
 148 a variety of situations and to gain an understanding of how the algorithm should  
 149 perform for experimental data. Simulations are used as opposed to training data  
 150 sets to better cover a complete range of possible situations.

### 151 3.1 Performance metrics

152 Identification of a data block contaminated with noise is a binary classification  
 153 problem where the data block is either a transient, contaminated block or a sta-

154 tionary, uncontaminated block. Thus, performance metrics used to evaluate binary  
155 classifiers can be used here (Ting 2010). Note that for this study, classification of  
156 a data block as a transient, along with its subsequent rejection by the method and  
157 removal of the data block from the set of interest is considered as a positive result.  
158 The associated negative result is the classification of a data block as stationary.  
159 This study considers three performance metrics: accuracy, false positive rate, and  
160 false negative rate. The *accuracy* is the fraction of test cases that are correctly  
161 classified as either a transient data block or a stationary data block. The *false*  
162 *positive rate* is the fraction of the total number of stationary data blocks that are  
163 incorrectly classified as transient data blocks. It provides a measure of reduction in  
164 useful, stationary data blocks due to the classification process. The *false negative*  
165 *rate* is the fraction of the total number of transient blocks that are misclassified  
166 as stationary data blocks and provides a measure of the contaminated data blocks  
167 that are allowed through the algorithm.

168 An intermediate step for computing the accuracy, false positive rate, and false  
169 negative rate is the calculation of the confusion matrix. For a binary classification  
170 problem, the confusion matrix is a two by two table containing the counts of the  
171 classifier output for true positives and true negatives on the diagonal elements and  
172 false positives and false negatives on the off-diagonal elements. Thus, the accuracy  
173 is the sum of the diagonal elements divided by the total number of data blocks,  
174 while the false positive rate and false negative rate are the off-diagonal elements  
175 divided by the total number of true or known positives or negatives, respectively.

### 176 3.2 Simulation cases

177 The desired measured signal and the contamination signal are modeled as inde-  
178 pendent Gaussian noise signals with different variances, with the variance of the  
179 contamination larger than the variance of the desired signal. Five parameters are  
180 studied in simulations. These are the ratio of the variance of the contamination to  
181 the variance of the signal, the total number of data blocks, the number of points  
182  $N$  in each data block, the percentage of the data blocks contaminated, and the  
183 percentage of the points in each data block that are contaminated. For all simu-  
184 lation cases, the total number of data blocks is swept through values of 100, 200,  
185 300, 400, 500, and 1,000. The remaining parameters are given in Table 1. These  
186 combinations yield a total of 132 individual simulation cases.

### 187 3.3 Simulation procedure

188 The simulation procedure is as follows. First, a simulation case is selected, and the  
189 case parameters are noted. Next, the noncontaminated signal is modeled as a unit  
190 variance Gaussian random signal with the number of data points per data block  
191 and the number of blocks specified for the simulation case. Next, the clean signal is  
192 divided into the desired number of blocks, with no block overlap. Then, the desired  
193 number of blocks are contaminated for the desired percentage of points (selected  
194 as the first part of the block) with additive noise specified by the variance ratio  
195 and added to the the block. The transient classification algorithm is applied to the  
196 simulated data, and the data blocks classified as transients are logged. For these  
197 simulations, the transient classification procedure automatically considers the 20%  
198 of data blocks with the lowest variance to be stationary because lower total block

Table 1. Parameter values for simulation cases. All cases sweep through six values of the total number of data blocks of 100, 200, 300, 400, 500, and 1000.

| <b>Variance ratio</b> | <b>Points per data block</b> | <b>Percentage of data blocks contaminated</b> | <b>Percentage of points in each data block contaminated</b> |
|-----------------------|------------------------------|---|---|
| 2                     | 8192                         | 75  | 100   |
| 2                     | 8192                         | 50  | 100   |
| 2                     | 8192                         | 25  | 100   |
| 2                     | 8192                         | 25  | 50  |
| 2                     | 8192                         | 25  | 25  |
| 2                     | 8192                         | 75  | 50  |
| 2                     | 8192                         | 75  | 25  |
| 2                     | 2048                         | 75  | 25  |
| 2                     | 2048                         | 75  | 100   |
| 2                     | 2048                         | 25  | 25  |
| 2                     | 2048                         | 25  | 100   |
| 3                     | 8192                         | 25  | 25  |
| 5                     | 2048                         | 25  | 100   |
| 5                     | 2048                         | 75  | 100   |
| 5                     | 2048                         | 25  | 25  |
| 5                     | 2048                         | 75  | 25  |
| 5                     | 8192                         | 75  | 25  |
| 5                     | 8192                         | 75  | 100   |
| 5                     | 8192                         | 25  | 25  |
| 5                     | 8192                         | 25  | 100   |
| 10                    | 8192                         | 25  | 25  |
| 100                   | 8192                         | 25  | 25  |

199 counts approach the minimum necessary for a reasonable autospectral estimate.  
 200 The confusion matrix elements are then calculated and recorded. The process is  
 201 repeated for a total of 50,000 trials of data generation for each simulation case. The  
 202 individual elements of the confusion matrix are examined to ensure the mean and  
 203 standard deviation have converged to within 0.1% based on the values from one  
 204 iteration to the next. Finally, the mean estimate for the confusion matrix is used  
 205 to compute the estimated mean accuracy, false positive rate, and false negative  
 206 rate for the simulation case.

### 207 3.4 Results

208 Table 2 presents a statistical summary of the three performance metrics over all  
 209 of the simulation cases. The accuracy ranges from 80.1% to 99.3%. However, if the  
 210 number of blocks is greater than or equal to 300, which is desirable for averaging  
 211 of the spectral estimate as it approaches a normalized random error of 5%, the  
 212 mean accuracy is greater than 90%. This condition also further constrains the  
 213 false positive rate bounds to range from 0.9% to 12.9%, and the false negative  
 214 rate bounds to range from 0.0% to 2.0%, improving on the results summarized in  
 215 Table 2.

Table 2. Statistical summary of performance metrics for all simulation cases.

|                | <b>Accuracy (%)</b> | <b>FPR (%)</b> | <b>FNR (%)</b> |
|----------------|---------------------|----------------|----------------|
| <b>minimum</b> | 80.1                | 0.9            | 0.0            |
| <b>mean</b>    | 94.4                | 8.8            | 0.3            |
| <b>median</b>  | 97.0                | 6.2            | 0.01           |
| <b>maximum</b> | 99.3                | 26.4           | 4.2            |

216 To assess the behavior of the algorithm, and example plot of  $|K|$  as a function of  
 217 block count is shown in Fig. 2. Here a global minimum is observed when 749 of the  
 218 blocks are retained, which is very close to the true number of 750 uncontaminated  
 219 blocks. Note that the accuracy is less than that expected for 999/1000 correct  
 220 classifications due to false positives and negatives, as discussed further below.  
 221 Also note that some noise is present at extremely low block counts. This points  
 222 back to the comment in Section 2 to set a minimum number of retained blocks.

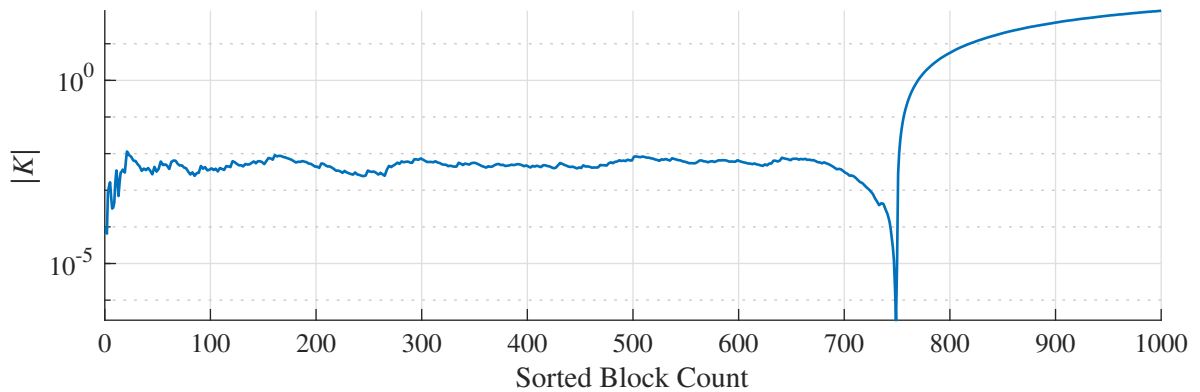


Fig. 2. Kullback-Leibler divergence as a function of included block count for a simulation with 1000 blocks of data, a variance ratio of 2, 8192 points per data block, 25% of the data blocks contaminated, and 50% of the points in each block contaminated.

### 223 3.4.1 Number of data blocks and variance ratio

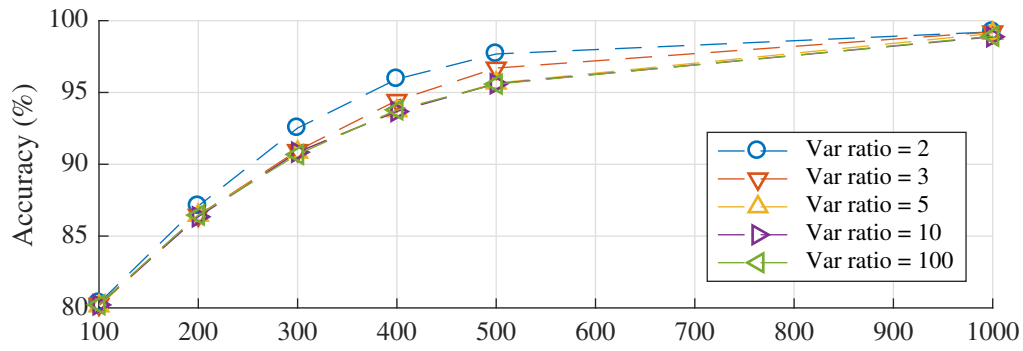
224 The variation in the performance of the algorithm is studied as a function of  
 225 the total number of data blocks and contamination to the signal variance ratio.  
 226 Here, the number of data points per block was held to  $N = 8,192$  points, the

227 percent of contaminated blocks to 25%, and the percent of each contaminated  
228 block perturbed to 25%. This resulted in 30 simulation scenarios selected from the  
229 132 total cases. The results, as plotted in Fig. 3, show that all performance metrics  
230 converge as a function of variance ratio when the ratio is greater than five. The  
231 accuracy and the false positive rate improve as the total number of data blocks  
232 increases. The false negative rate shows more variation, but the values are below  
233 0.14% for all 30 scenarios. These rates correspond to total false negative counts of  
234 zero, one, or, at worst, two misclassified blocks.

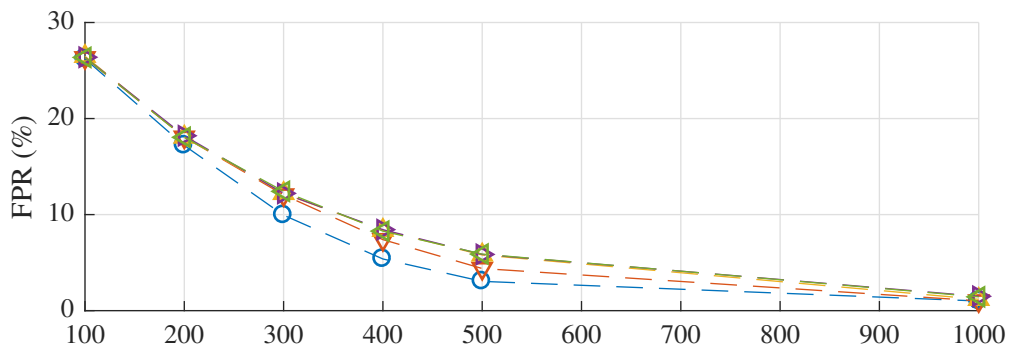
#### 235 *3.4.2 Percent of contaminated block perturbed*

236 In the actual experiments analyzed in a subsequent section, transient gust con-  
237 tamination occurs sporadically and for short durations. Thus, for any data block  
238 that is impacted, only a portion of that block may be contaminated. Understand-  
239 ing how sensitive the performance metrics are to the percentage of any given data  
240 block that is perturbed is critical to assessing the robustness of the method. This  
241 simulation subset held the variance ratio to 2 (the most challenging value in the  
242 simulation study), the number of data points per block to  $N = 8,192$  points, and  
243 the percentage of contaminated blocks to 25%. This resulted in 18 simulation sce-  
244 narios selected from the 132 total cases. The results, as plotted in Fig. 4, show that  
245 the accuracy and the false positive rate are minimally affected by the percentage  
246 of the contaminated data block that is perturbed, especially when compared to the  
247 impact from the total number of data blocks. The magnitudes of the correlation  
248 coefficients between the accuracy and percentage of the data block contaminated,  
249 and between the false positive rate and the percentage of the data block contam-  
250 inated are less than 0.1, confirming the lack of a linear relationship as seen in

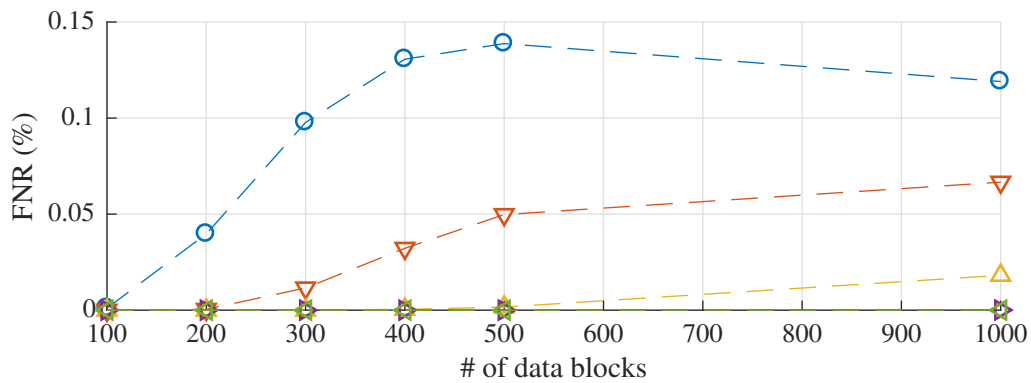




(a) accuracy



(b) FPR



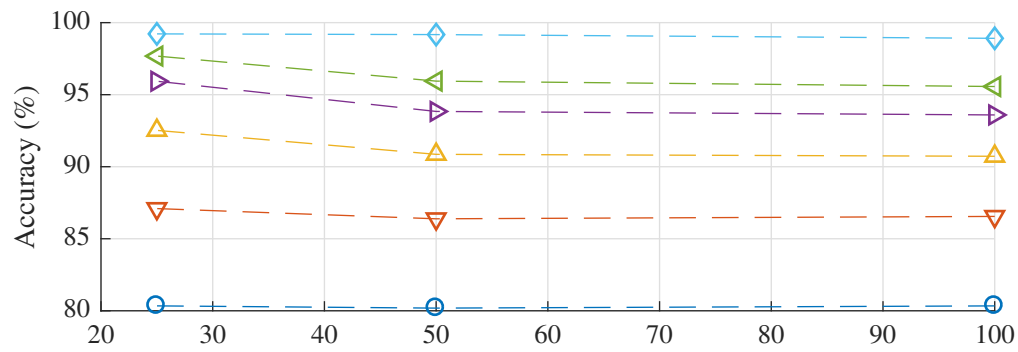
(c) FNR

Fig. 3. Performance metrics varying the total number of data blocks and the contamination to signal variance ratio. The number of data points per block is held to to  $N = 8,192$  points, the percentage of contaminated blocks to 25%, and the percent of each contaminated data block perturbed to 25%.

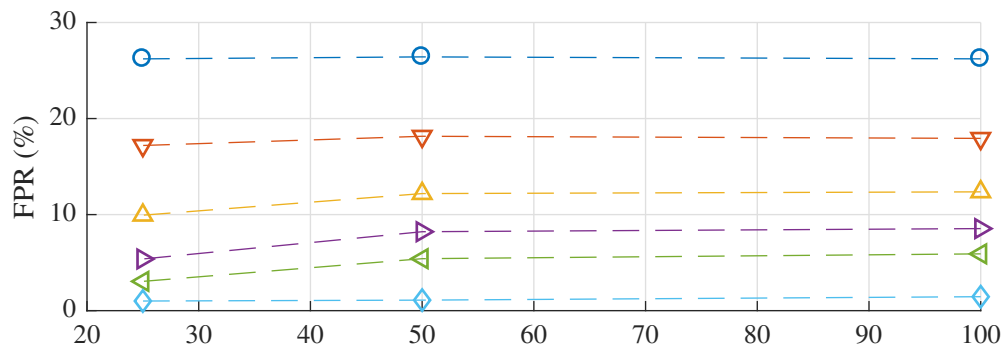
251 Fig. 4. However, the false negative rate does show a functional dependence on the  
252 percentage of the data block contaminated. This has a correlation coefficient of  
253  $-0.25$  (p-value of 0.004). Thus, as the percentage of the data block that is contam-  
254 inated increases, the method can more easily identify data blocks that have been  
255 contaminated. However, the maximum false negative rate is still only 0.14%.

### 256 *3.4.3 Percent of data blocks that are contaminated*

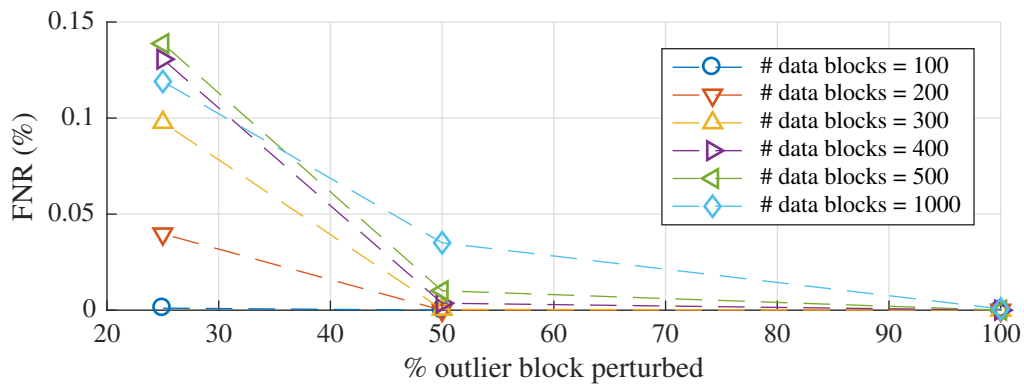
257 The variation in the performance of the classification algorithm is studied as a  
258 function of the percentage of data blocks that are contaminated. This simula-  
259 tion subset held the variance ratio to 2, the number of data points per block to  
260  $N = 8,192$  points, and the percent of each contaminated block perturbed to 25%,  
261 resulting in 18 simulation scenarios selected from the 132 total cases. The results,  
262 as plotted in Fig. 5, show that the accuracy and false positive rate improve with  
263 an increasing percentage of transient blocks in the total data set, whereas the false  
264 negative rate worsens. The values of all three performance metrics as a function  
265 of the percentage of contaminated blocks present in the total data set are also im-  
266 pacted by the total number of data blocks. However, when there is a total of 1,000  
267 data blocks, the variation in the performance metrics as a function of the percent-  
268 age of contaminated data present is minimal. With at least 300 total blocks, as  
269 might be recommended, the variation is greatly reduced. Note that a critical value  
270 of the percentage of contaminated blocks appears to exist between 50% and 75%  
271 where the behavior of the performance metrics changes.



(a) accuracy

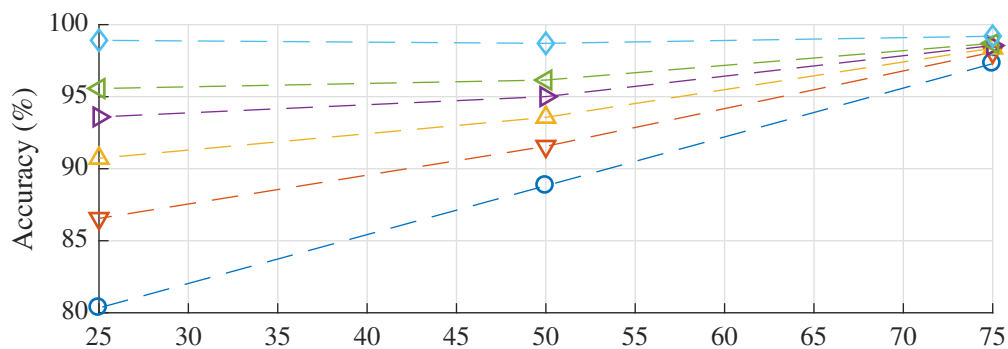


(b) FPR

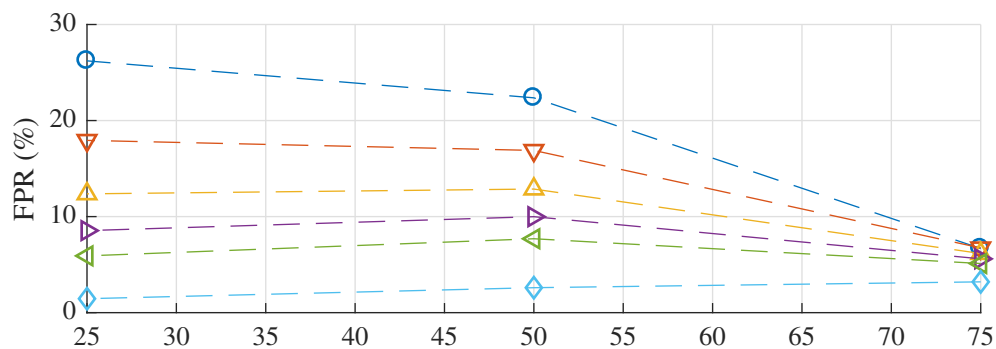


(c) FNR

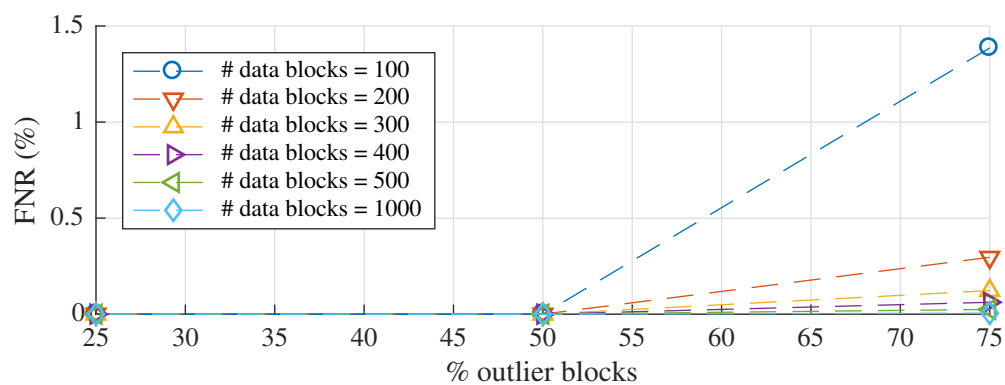
Fig. 4. Performance metrics varying the percentage of the contaminated block that is perturbed from the contamination signal while holding the variance ratio to 2, the number of data points per block to  $N = 8,192$  points, and percentage of contaminated blocks to 25%.



(a) accuracy



(b) FPR



(c) FNR

Fig. 5. Performance metrics varying the percent of data blocks that are contaminated while holding the variance ratio to 2, the number of data points per block to  $N = 8,192$  points, and percentage of the data points in the data block perturbed by contamination to 25%.

## 272 **4 Experimental Results**

273 The transient classification procedure is applied to an advanced aircraft noise  
274 study conducted at the NASA Langley Research Center's 14- by 22-Foot Subsonic  
275 Tunnel (Heath et al. 2016). A photograph of an example test configuration from  
276 this study is shown in Fig. 6, where a hybrid wing body model is installed inverted  
277 in the facility test section. As shown in the photograph, microphones are installed  
278 on sideline traversing towers, as well as a truss and array panel located above the  
279 facility test section.

280 The NASA Langley 14- by 22-Foot Subsonic Tunnel is, by design, an aerody-  
281 namic wind tunnel, which can operate in an open test section configuration. While  
282 significant acoustic improvements have been applied to the facility, measurement  
283 microphones are, under some installation configurations, close enough to the open-  
284 jet shear layer that hydrodynamic gusts may contaminate the out-of-flow acoustic  
285 measurements. This was primarily observed when microphones were at the far-  
286 downstream end of the test section, although occasional gust impingement was  
287 seen at other measurement stations.

288 An extreme example of gust impingement from the airframe noise component  
289 of the test is shown in Fig. 7. The plotted data are for an acquisition where one of  
290 the speakers embedded in the model body was driven with a random noise signal  
291 that was bandpass filtered to span a frequency range of 4 kHz to 16 kHz. The  
292 speaker data are used rather than the model's isolated airframe noise data as, in  
293 the frequency domain, these data provide a more clear visual representation of the  
294 influence of transient contamination over a limited bandwidth due to more distinct  
295 spectral structures.

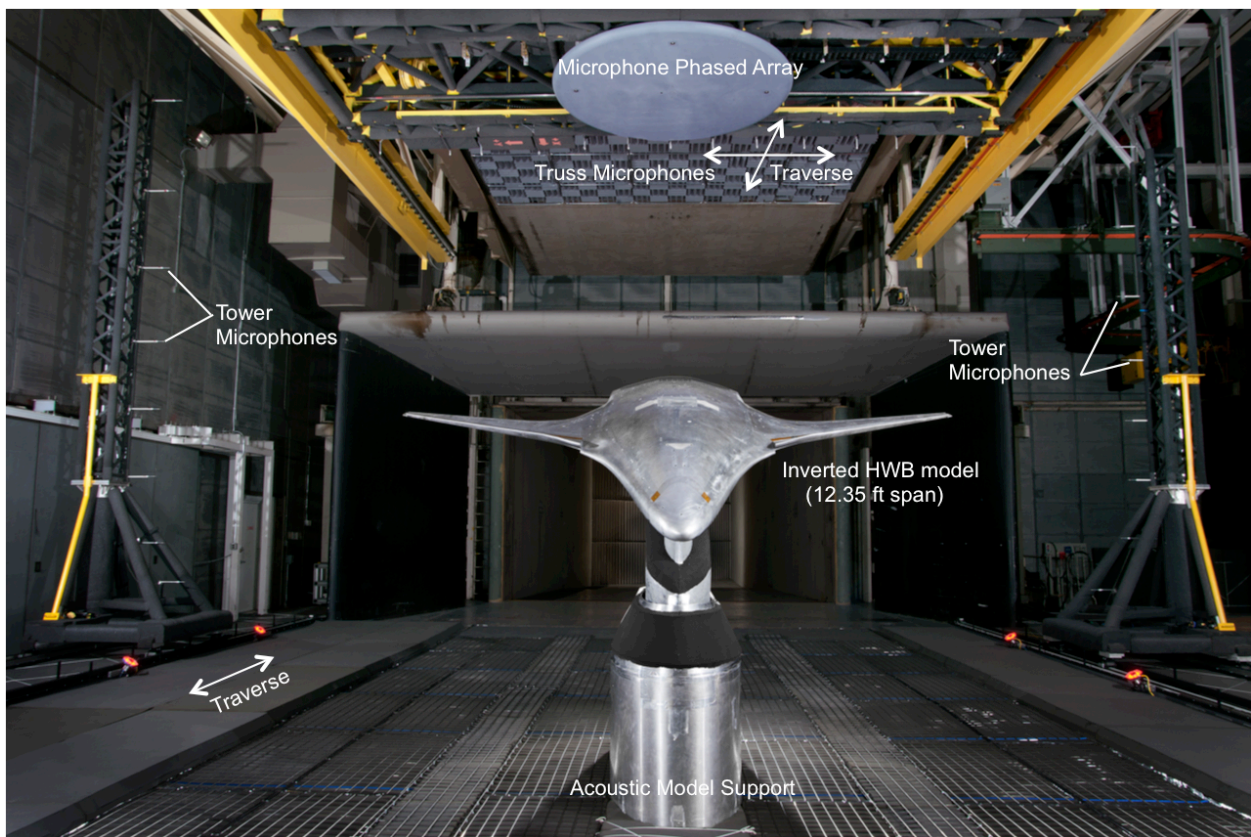


Fig. 6. Example arrangement of a hybrid wing body model, phased array and tower traverses installed in the NASA Langley 14- by 22-Foot Subsonic Tunnel.

296 The hybrid wing body model was pitched to an angle of attack of  $14.5^\circ$ , and  
 297 the test section Mach number was  $M = 0.23$ . The acoustic measurement hardware  
 298 was traversed to the far-downstream end of the test section. As shown by the  
 299 time series in Fig. 7a, the array center microphone signal appears as might be ex-  
 300 pected for a stationary, band-limited random signal. The south tower microphone,  
 301 located in the upper-right-hand corner of the picture in Fig. 6, clearly experiences  
 302 extreme transient bursts as shown in Fig. 7b. The corresponding autospectra are  
 303 shown in Figs. 7c and 7d. While the array center microphone spectrum shows the

304 low frequency content of the signal at 4 kHz, the south tower microphone spec-  
305 trum is masked by the low frequency content of the burst. Note that at this stage  
306 of processing, two clean signals would not overlay due to differences in propaga-  
307 tion distance between the source and each microphone, along with the speaker  
308 directivity. Also, this test is a prime example of why an automated classification  
309 method is desirable. The contamination in the data is clear and could readily be  
310 separated manually. However, roughly a quarter of a million time series records  
311 were generated during the test. Manual inspection of such a volume of data is  
312 unreasonable.

313 For these data, the procedure developed for transient classification is applied  
314 by breaking the microphone time series into 920 blocks of desired length  $N = 8192$   
315 points. This corresponds to the baseline processing parameters used in the test for  
316 spectral analysis (Bahr et al. 2014). The minimum number of accepted blocks is  
317 set to 100 based on observation of the spectral convergence. A histogram of the  
318 south tower microphone data block variances is shown with respect to the left  
319 axis in Fig. 8, with the 16 most energetic blocks removed from the plot. Even  
320 without these blocks, which would extend the plot abscissa beyond a variance of  
321  $500 \text{ Pa}^2$ , this histogram shows a long, thin tail in the direction of large variance  
322 values. The corresponding probability density functions for the median- and mean-  
323 based models are shown with respect to the right axis in the figure. Note that the  
324 bandwidth parameter  $B$  for these data is extremely low, generally between  $4 \times 10^{-3}$   
325 and  $5 \times 10^{-3}$  depending on the included blocks. This is due to the high levels of  
326 low frequency data, below the speaker operating range.

327 Of the 920 input blocks, 567 are rejected. The computed  $|K|$  as a function of  
328 block count used to separate the blocks is plotted in Fig. 9, showing an obvious

329 minimum as it did with the simulated data in the previous section. The almost-  
330 monotone increase at higher block counts is similar in behavior to the  $|K|$  plot for  
331 simulated data, and appears to be associated with data convergence. The series  
332 of local minima near the global minimum are not easily explained, as the baseline  
333 variances, variance means, and variance medians are all reasonably smooth. It  
334 is only when differences and ratios of these parameters are computed that more  
335 jagged features appear.

336 It should be noted that while 567/920 blocks is a large portion of the data  
337 to reject, this microphone acquisition is from a location normally outside of the  
338 bounds of reasonable acoustic measurement positions in the facility. The histogram  
339 of the remaining block variances is shown in Fig. 10, along with the median- and  
340 mean-based probability density function estimates for the retained block set. As  
341 expected, the probability density functions overlay for the minimum value of  $|K|$ ,  
342 indicating near-total agreement between the mean and median models and that all  
343 the data blocks provide useful information to the statistics. The outliers, as mod-  
344 eled, have been eliminated. The output of the procedure is shown in Figs. 11a and  
345 11b. Visually, the technique has identified and removed the obvious contamination  
346 from the time series. In the spectral analysis, the 4 kHz content of the signal is  
347 now visible, with a reduction of up to 10 dB in the microphone autospectrum at  
348 lower frequencies. Higher frequencies are unaffected.



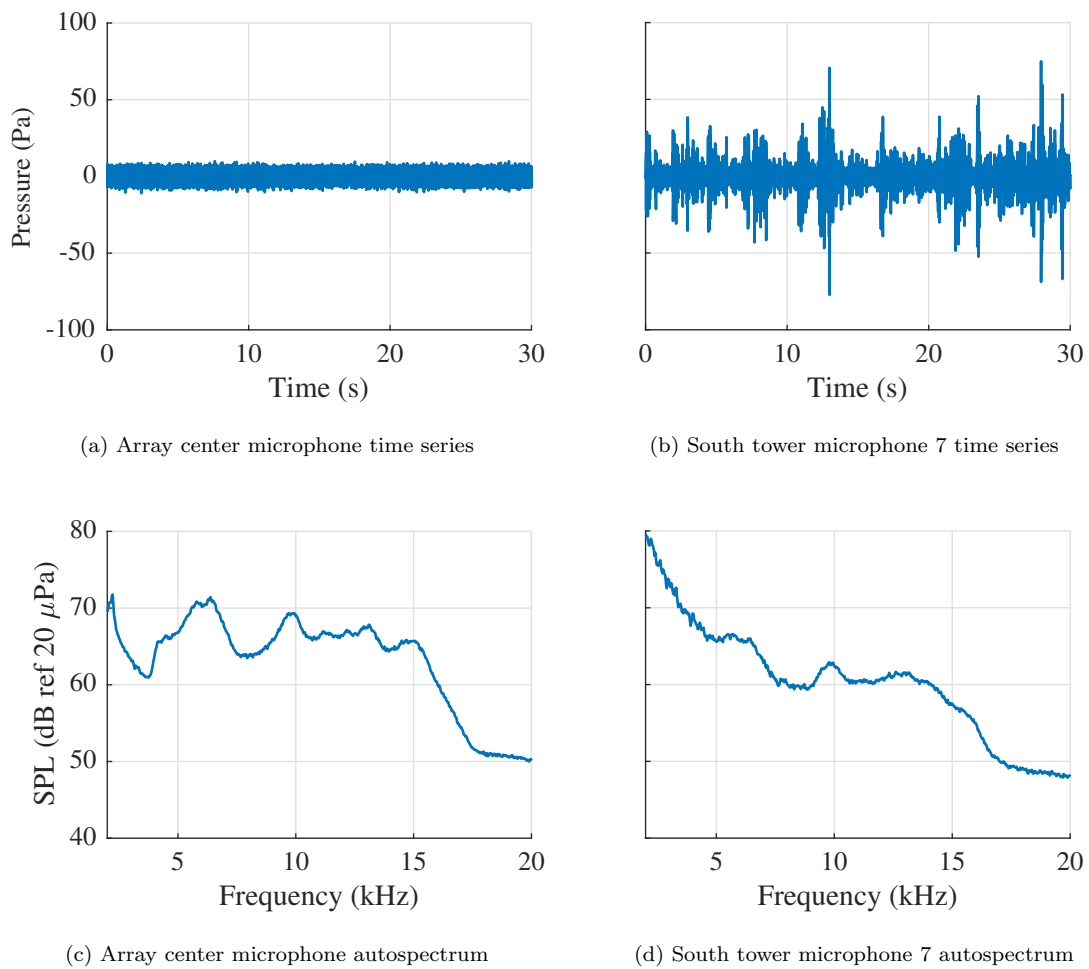


Fig. 7. Example data contamination by hydrodynamic impingement. The two compared microphones observed a calibration signal with an output band of 4 kHz to 16 kHz, emitted by one of the model embedded speakers. The hybrid wing body model was at an angle of attack of  $14.5^\circ$ , and the test section Mach number was  $M = 0.23$ . Acoustic hardware were at the far downstream traverse location. Spectral binwidths are 30.5 Hz.

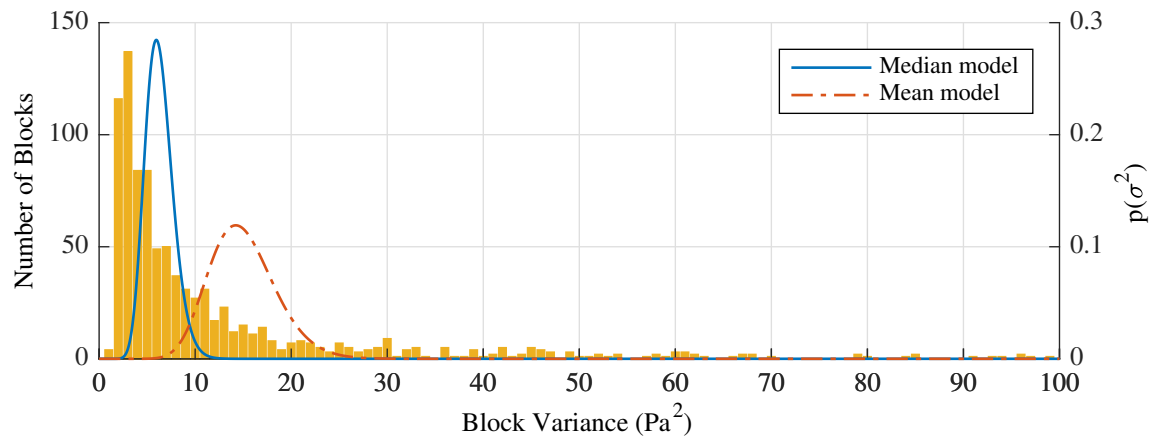


Fig. 8. Histogram of block variances from the south tower time series in Fig. 7 excluding the 16 most energetic blocks, and modeled data probability density functions.

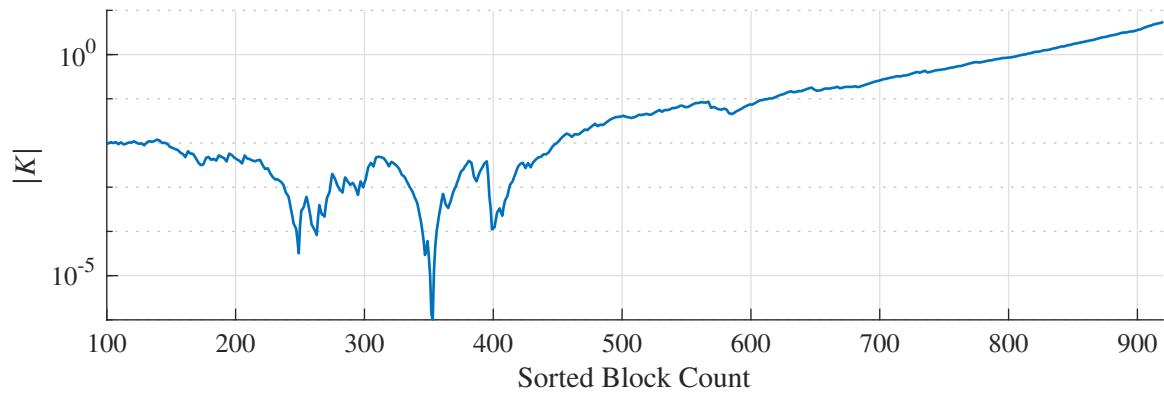


Fig. 9. Kullback-Leibler divergence as a function of included block count for the south tower time series data.

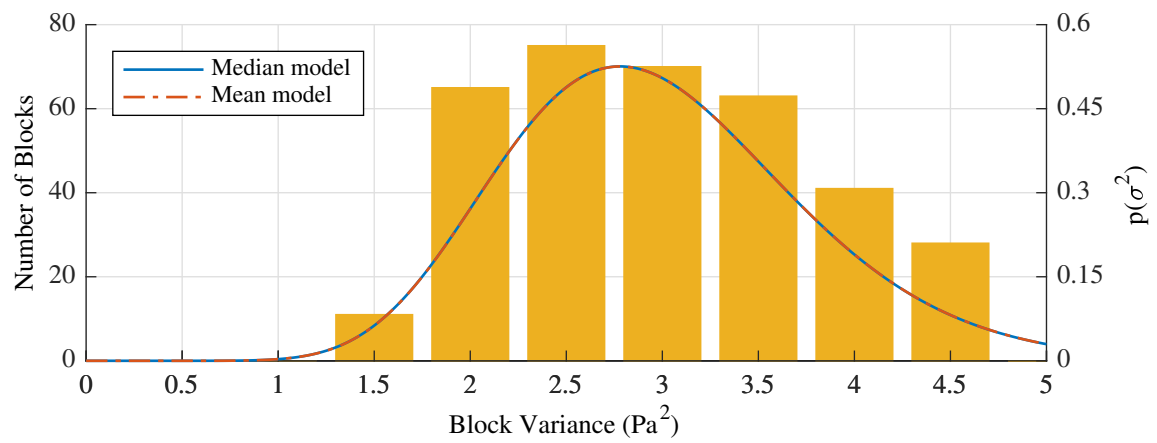
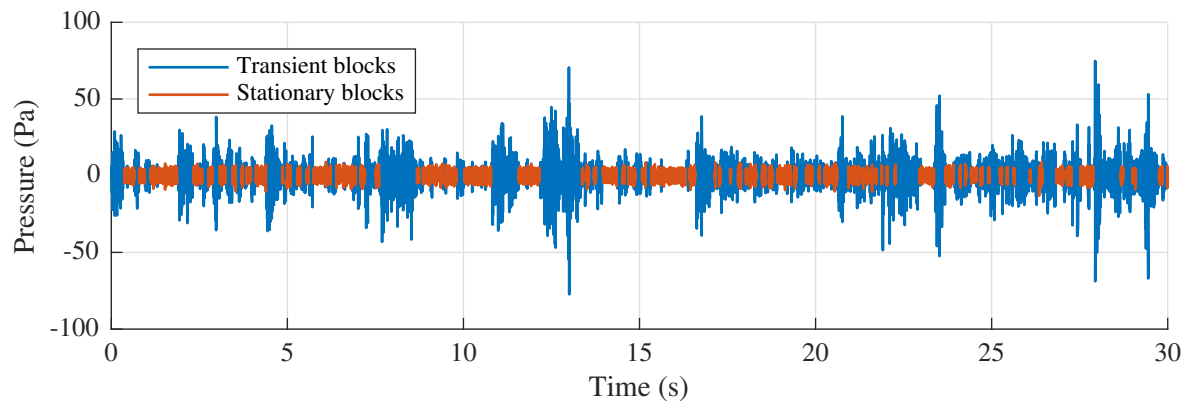
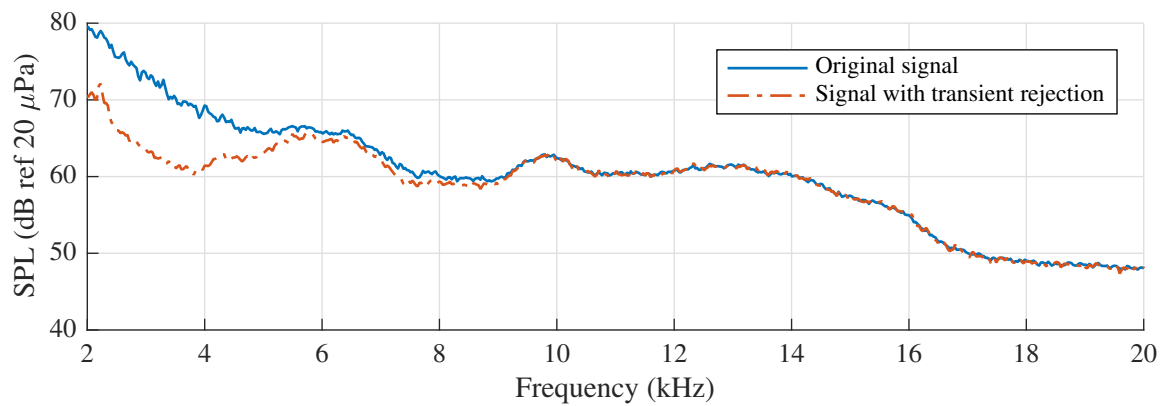


Fig. 10. Post-classification histogram of south tower time series data from Fig. 8, along with post-rejection models (mean model almost completely overlays the median model).



(a) Blocks accepted and rejected by the algorithm



(b) Effect of transient block rejection on microphone autospectrum

Fig. 11. Results of transient rejection algorithm when applied to the south tower time series data from Fig. 7b. Data blocks are plotted as a function of time. The shift in the estimated data autospectrum is shown. Spectral binwidths are 30.5 Hz.

## 349 5 Summary & Conclusions

350 An automated method for classifying transient data segments that contaminate  
351 stationary acoustic data is presented. The method requires two assumptions. First,  
352 it treats the underlying stationary signal of interest as having Gaussian random  
353 characteristics. Second, it assumes that contaminated segments of data will have  
354 higher variance than clean segments of data. Under these assumptions, it is an  
355 unsupervised method that performs binary classification: either a data block is  
356 contaminated by a transient signal or it is clean.

357 An extensive set of simulations covering a broad range of conditions shows that  
358 the technique has a high degree of accuracy as long as at least 300 data blocks are  
359 used, though 500 may be preferable. The FPR may still be greater than 5% under  
360 some of the simulated circumstances. However, falsely classifying a few blocks of  
361 stationary data as transient and discarding them is not problematic. Wind tunnel  
362 time is expensive, so data records have a practical duration limit based on cost.  
363 Regardless, standard spectral estimation techniques will still perform well if a few  
364 extra blocks are discarded while hundreds are retained. Simulations suggest the  
365 technique has a very low FNR for the parameter space explored, so misclassifying  
366 enough transient data as stationary to noticeably contaminate a spectral estimate  
367 is unlikely.

368 Experimental results from a worst-case scenario in an aeroacoustic wind tunnel  
369 test show that, visually, the method succeeds in separating contaminated blocks  
370 from the baseline signal of interest. Spectral estimation of the signal both before  
371 and after the application of the technique shows up to a 10 dB improvement in  
372 signal-to-noise ratio due to the removal of contamination. Features in the acoustic

spectrum that are masked in the baseline data set are revealed once the transient blocks are removed.

**Acknowledgements** The authors would like to acknowledge the support provided by the 14-foot by 22-foot Subsonic Tunnel team, by colleagues in the Aeroacoustics and Advanced Sensing & Optical Measurements branches at the NASA Langley Research Center, and by colleagues in the Aerodynamics, Noise, and Propulsion Laboratory in the Boeing Test & Evaluation organization at The Boeing Company. The hybrid wing body test was funded by the NASA Environmentally Responsible Aviation Project.

## References

- Aggarwal CC (2017) *Outlier Analysis*, 2nd edn. Springer, New York, NY
- Bahr CJ, Horne WC (2017) Subspace-based background subtraction applied to aeroacoustic wind tunnel testing. *International Journal of Aeroacoustics* 16(4-5):299–325
- Bahr CJ, Brooks TF, Humphreys WM, Spalt TB, Stead DJ (2014) Acoustic Data Processing and Transient Signal Analysis for the Hybrid Wing Body 14-foot by 22-foot Subsonic Wind Tunnel Test. 20<sup>th</sup> AIAA/CEAS Aeroacoustics Conference, AIAA Aviation 2014, Atlanta, GA, 2014, AIAA 2014-2345
- Bendat JS, Piersol AG (2000) *Random Data Analysis and Measurement Procedures*. John Wiley & Sons, Inc., New York, NY
- Cardoso J (1997) Infomax and maximum likelihood for blind source separation. *IEEE Signal Processing Letters* 4(4):112–114
- Coleman HW, Steele WG (1999) *Experimentation and Uncertainty Analysis for Engineers*, 2nd edn. John Wiley & Sons, Inc., New York, NY
- Hawkins D (1980) *Identification of Outliers*. Springer, New York, NY

- 397 Heath SL, Brooks TF, Hutcheson FV, Doty MJ, Bahr CJ, Hoad D, Becker LE,  
398 Humphreys WM, Burley CL, Stead DJ, Pope DS, Spalt TB, Kuchta DH, Plass-  
399 man GE, Moen JA (2016) NASA Hybrid Wing Body Aircraft Aeroacoustic Test  
400 Documentation Report. Tech. Rep. NASA TM-2016-219185
- 401 Humphreys WM, Brooks TF, Hunter WW, Meadows KR (1998) Design and Use  
402 of Microphone Directional Arrays for Aeroacoustic Measurements. 36<sup>th</sup> AIAA  
403 Aerospace Sciences Meeting & Exhibit, Reno, NV, 1998, AIAA-98-0471
- 404 NIST (2013) NIST/SEMATECH e-Handbook of Statistical Methods, chap  
405 1.3.6.6.11. Gamma Distribution. URL [http://www.itl.nist.gov/div898/  
406 handbook/](http://www.itl.nist.gov/div898/handbook/)
- 407 Soderman PT, Allen CS (2002) Microphone measurements in and out of airstream.  
408 In: Mueller TJ (ed) Aeroacoustic Measurements, Springer-Verlag, Berlin, Hei-  
409 delberg, New York, chap 1, pp 22–24
- 410 Ting KM (2010) Confusion matrix. In: Sammut C, Webb GI (eds) Encyclopedia  
411 of Machine Learning, Springer US, Boston, MA, p 209
- 412 Zelen M, Severo NC (1972) Probability functions. In: Abramowitz M, Stegun IA  
413 (eds) Handbook of Mathematical Functions, Dover Publications, Inc., New York,  
414 chap 26, pp 940–943
- 415 Zhang J (2013) Reducing bias of the maximum likelihood estimator of shape pa-  
416 rameter for the gamma distribution. Computational Statistics 28(4):1715–1724